Multimodal imaging shows fibrosis architecture and action potential dispersion are predictors of arrhythmic risk in spontaneous hypertensive rats

Supporting Image and Cell Segmentation Information

Prashanna Khwaounjoo,[1] Gregory B. Sands,[1] Ian J. LeGrice,[1,2] Girish Ramulgun,[1,3] Jesse A. Ashton,[1,2] Johanna M. Montgomery,[2] Anne M. Gillis,[4] Bruce H. Smaill,[1] Mark L. Trew[1]

[1]Auckland Bioengineering Institute, University of Auckland, Auckland, New Zealand; [2]Department of Physiology, University of Auckland, Auckland, New Zealand; [3]IHU-Liryc, University of Bordeaux, Bordeaux, France; [4]Libin Cardiovascular Institute of Alberta, University of Calgary, Calgary, AB, Canada.

Anatomical measurements and fibrosis distribution

Tiled images of wheat germ agglutinin-conjugated AF488 (WGA)-labeled short axis sections of rat heart were combined with ImageJ (imagej.nih.gov) to create a single image. Figure 1A shows an example from an 18 month animal. Initial segmentation of tissue from non-tissue used a binary filter to obtain a mask for the short axis slice (Figure 1B). Measurements were taken of the average thicknesses of the LV and RV (Figure 1B) and lumen area and lumen centroid (Figure 1C).

Cell membranes and the extracellular matrix are labeled by WGA. Greater image intensity within the boundary mask indicates the presence of fibrosis (Figure 1A), while the spatial distribution of this signal provides information on the nature and extent of this fibrosis. Using a maximum entropy intensity filter[1] the higher intensity pixels were segmented to differentiate the regions of fibrosis from the rest of the tissue and create a mask (Figure 1D). This filter was chosen as it was able to duplicate the histogram based WGA fibrosis segmentation from Emde et al. (2014).[2] For all hearts, the total segmented area of fibrosis was normalised with respect to short-axis area to determine the fibrotic percentage.

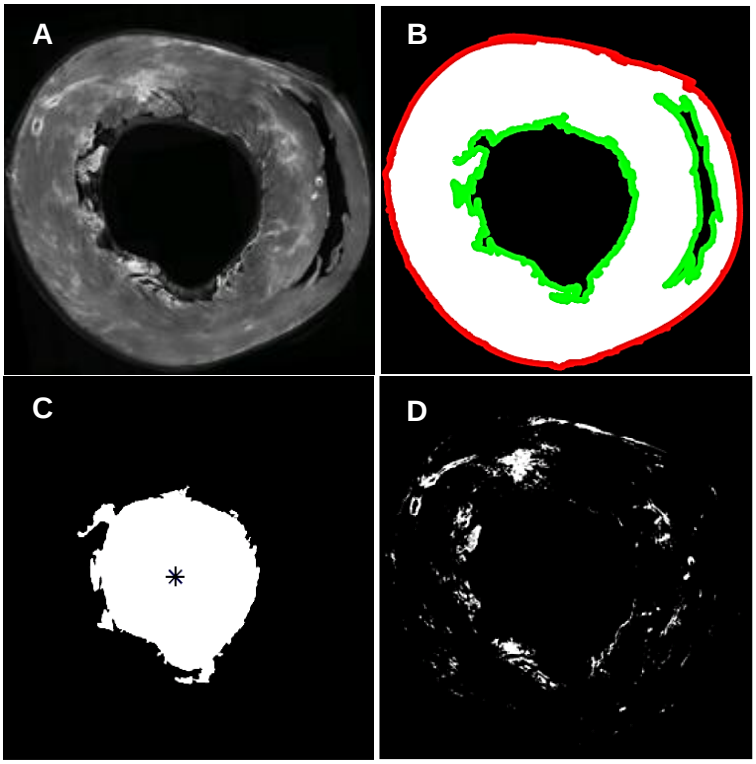

Figure 1. Short axis slice representation and measurements. **A.** Merged WGA stained short axis slice (higher intensity pixels indicate fibrosis) **B.** Tissue segmentation (white), endocardial (green) and epicardial (red) coordinates **C.** LV cavity with centroid highlighted by asterisk. **D.** Segmented patches of fibrosis.

To quantify and compare the distribution of fibrosis across all hearts, the segmented mask (Figure 1D) was translated into a polar coordinate system. For each separate individual patch in the mask (i.e. a patch of fibrosis – based on the WGA intensity signal), the patch centroid and area were computed. The centroid position was mapped into a polar coordinate system based on its polar angle and transmural (wall thickness) location relative to the lumen centroid (Figure 2A). A polar angle of 0^{o} was defined as mid septum and 90^{o} to 270^{o} were the LV free wall. In the transmural field 0 was the endocardium and 1 the epicardium. Local "densities" of the patches were then determined by discretizing the spatial field into 50 by 50 bins. The resultant field was smoothed using a 2D histogram filter[3] to create a "heat map" (Figure 2B).

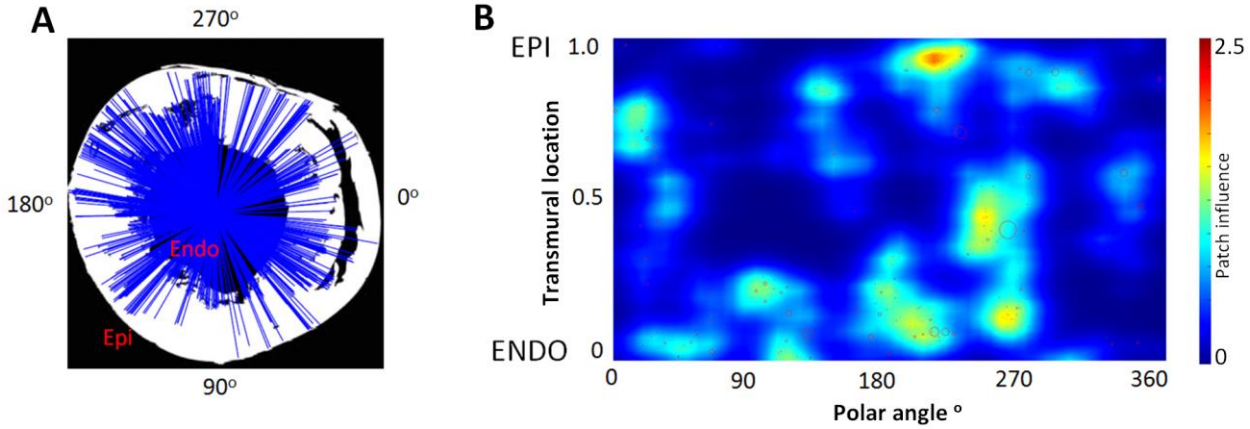

Figure 2. Fibrosis patch distribution and density. **A.** Intramural location of patches of fibrosis relative to LV cavity centroid. Blue lines indicate identification of patch from cavity centre. **B.** Heat map of fibrosis patch density in the polar coordinate system. Colour scale indicates influence of patch of fibrosis. Red indicates the influence of 2.5 or more patches and dark blue indicates no fibrotic influence.

The heat map was resampled to 100×360 pixels in the transmural and polar angle axes respectively. A threshold (using a value of 1, representing the influence of one patch) was applied to the resampled "heat map" image to quantify the influence of fibrosis patch density and extract the connected high-density regions. These aggregated regions of fibrosis patches from the heat map in Figure 2B are shown in Figure 3A as white regions. The regions were skeletonized, using the MATLAB® `bwskel`* function, as shown in Figure 3B and Figure 3C. The area of the region with the longest skeletonization (a measure of fibrotic patch density tortuosity and, hence, possible reentrant path length – referred to as the aggregated fibrosis patch density length (AFL)) was normalized across all hearts in the study giving an index between 0 and 1. This is the aggregated fibrosis patch density area (AFA) index.

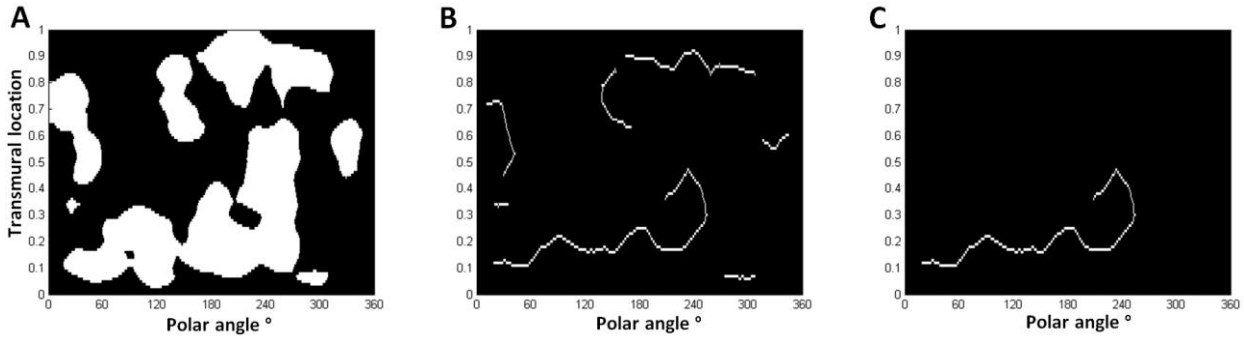

Figure 3. Mask of connected regions of fibrosis and measurements. **A.** Mask of connected regions of fibrosis (threshold of 1) **B.** Skeletonised lengths of each separate contiguous region of the mask **C.** Maximum path length of the skeletonised lengths.

This method for assessing the aggregation of fibrosis patch density in cardiac tissue ensures that the structure of the fibrotic patch distribution is correctly accounted for. Fibrotic structures as barriers to coordinated activation would not be fully captured by just a maximum area measure, for example. Our fibrotic consolidation measure includes both path length and area, and holds similarities to a measure of tortuosity in 2D discontinuous myocardium that was developed and used in the analysis of Engelman et al. (2010).[4]

Typical examples of the spatial distributions and characteristics of fibrosis quantified using this method applied to LV short axis slices are shown in Figure 4. The dark areas in Figure 4A are regions of intense WGA fluorescence due to perimysial or replacement fibrosis. The heterogeneous distribution of these patches is highlighted in the polar distribution maps (Figure 4B) and the analysis of fibrotic regional connectedness is shown in Figure 4C.

Each high intensity pixel (darker pixels in Figure 4A) was also translated into the polar coordinate field to quantify the distribution of the amount of fibrosis. The resulting image was discretized into 10 and 12 segments for the transmural and polar axes respectively (Figure 5).

* mathworks.com/help/images/ref/bwskel.html

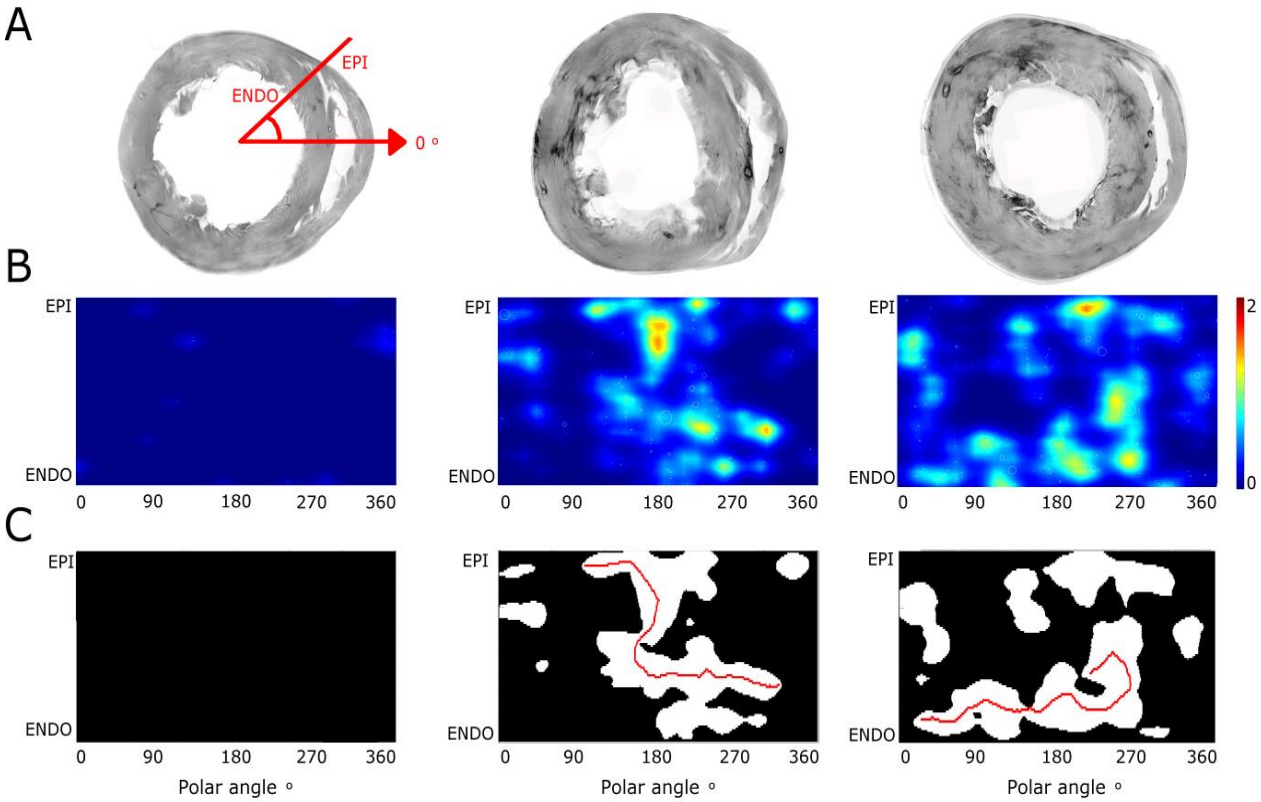

Figure 4. Typical distributions of WGA staining in LV short-axis sections at 6, 12 and 18 months. **A.** Initial LV sections, intensely dark regions stained are representative of patches of fibrosis. **B.** Polar heat maps reflect the intensity and regional extent and the distribution of patches of fibrosis. **C.** Characterisation of potentially connected regions of fibrosis (white). Maximum skeletonised lengths are indicated in red.

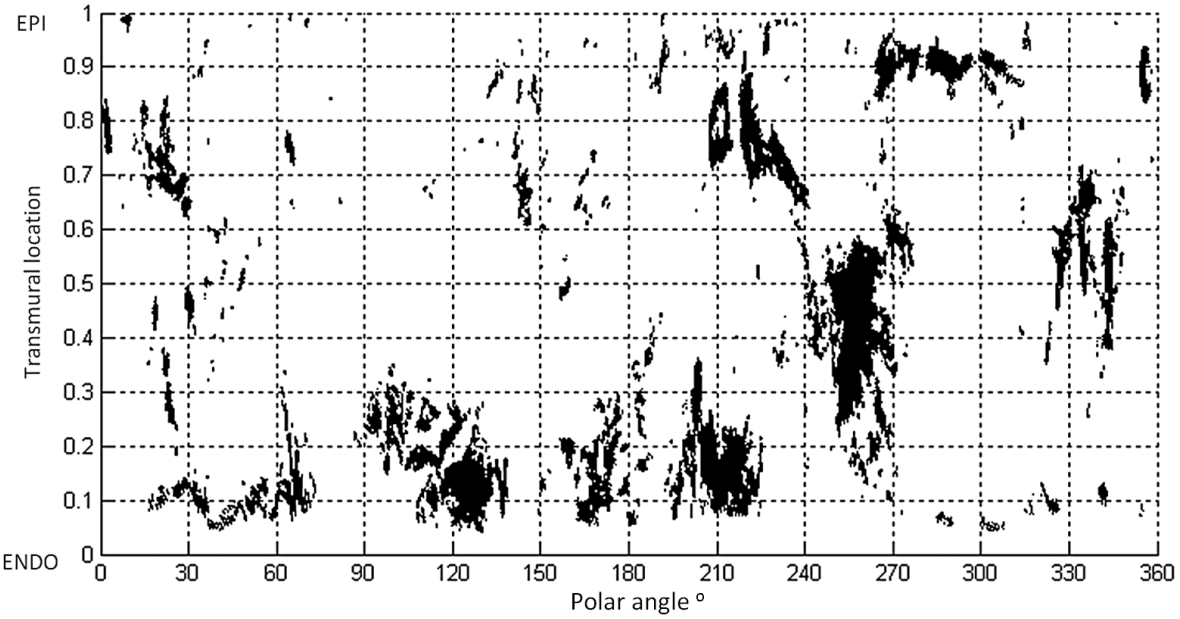

Figure 5. Distribution of fibrosis (individual high intensity pixels of WGA) in circumferential and transmural coordinate system. Transmural axes discretised into 10 sections of 0.1 units, while the circumferential axes have been discretised into 12 radial sections of 30 °. These data are equivalent to data in figures 1, 2, 3 and 4 column 3.

Cellular organization and architecture

ITK SNAP (itksnap.org)[5] was used to manually segment the high resolution cell data into individual cells (Figure 6). The segmentation was conducted by a contract operator with no link to the project and its potential findings (i.e. they were unaware of potential alterations to cell morphology with HHD progression). For each internal cell (i.e. a whole myocyte fully contained in the image volume) the longitudinal orientation was determined using the eigenvectors of the covariance matrix.[6] The longitudinal axis and centre of mass of the cell were then used to determine the cell cross sectional area. Cell lengths and total cell volumes were also measured, while the surface areas were calculated using Minkowski measures.[7] Distance maps from each internal (whole) myocyte were generated to identify/count all other myocytes within a distance of 1 voxel (0.41 μm) to the outer sarcolemma. This metric provided an estimate of likely cell coupling i.e. number of neighboring myocytes. The relative volume of the fibrosis was estimated from the WGA intensity using the ImageJ (imagej.nih.gov) implementation of the Shanbhag filter.

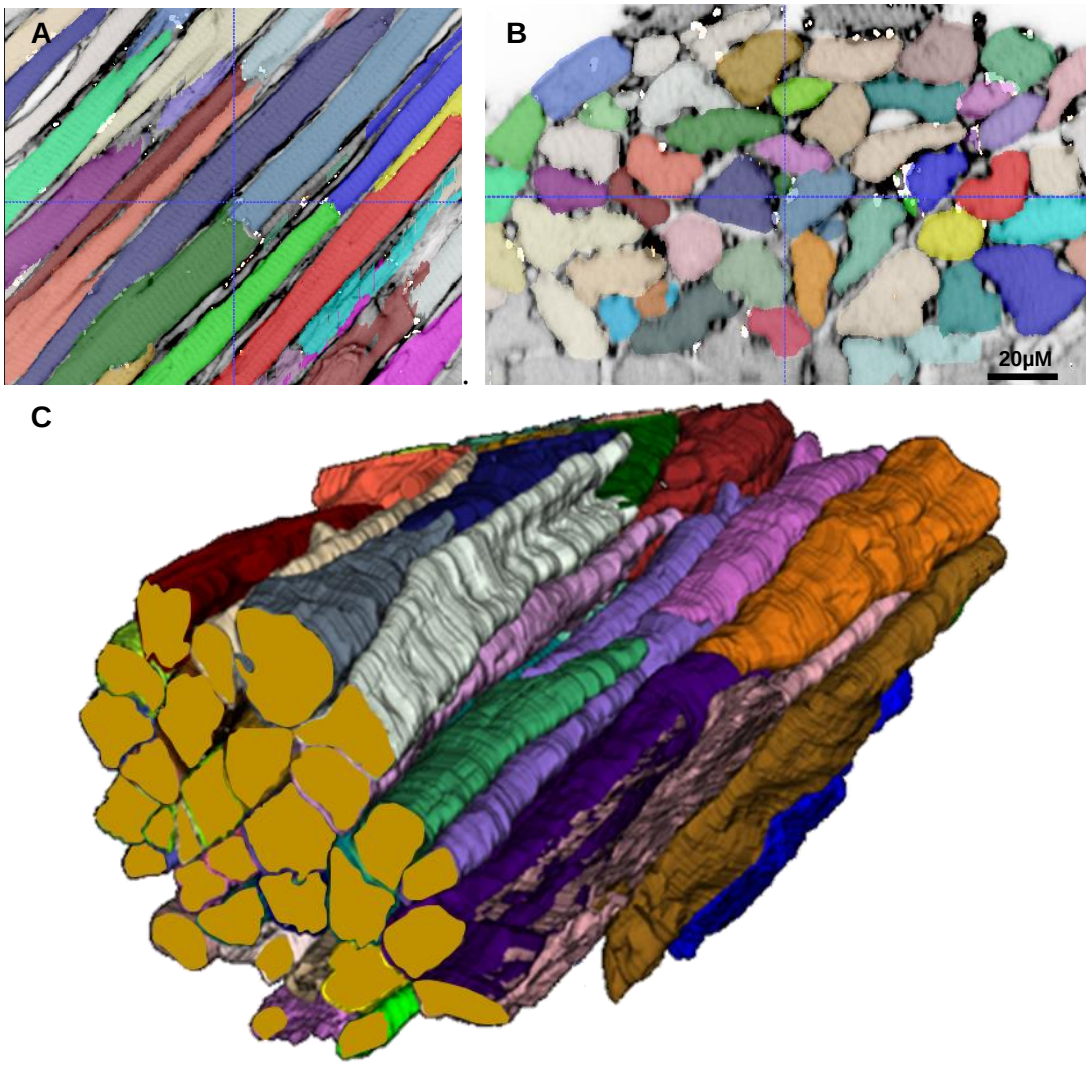

Figure 6. Cell segmentations using ITK SNAP. **A.** Axial slice of tissue volume. **B.** Side view of tissue section. **C.** 3D redering of segmented cells. Cells not wholly in the image volume are identified by their truncation at the image boundaries.

Table 1. Raw cell measurements across all intact cells from all animals.

Animal	Age (months)	Fibrosis %	Cell volume (μm^3)	Cell cross-section (μm^2)	Cell length (μm)	Surface area to volume ratio ($1/\mu m$)	Number of adjacent cells
1	12.2	6.5	35749	387	142	0.37	11
1	12.2	6.5	23243	336	94	0.37	10
1	12.2	6.5	27272	337	113	0.36	10
1	12.2	6.5	32623	319	132	0.33	8
1	12.2	6.5	14341	353	50	0.38	7
1	12.2	6.5	55673	528	153	0.26	10
1	12.2	6.5	52665	415	160	0.29	6
1	12.2	4.1	50087	470	156	0.28	9
1	12.2	4.1	58018	456	167	0.27	12
1	12.2	4.1	89969	587	200	0.23	10
2	12.4	11.9	81626	560	191	0.25	9
2	12.4	11.9	43487	320	133	0.33	9
3	12.4	13.8	30635	373	105	0.26	6
3	12.4	10.6	65641	616	133	0.21	8
5	12.6	25.0	77100	787	133	0.21	3
8	5.9	2.8	84866	519	204	0.22	8
8	5.9	2.8	83639	364	274	0.25	13
8	5.9	2.8	60826	346	225	0.28	8
8	5.9	2.8	51844	241	259	0.31	5
8	5.9	2.8	63121	392	193	0.27	7
9	6.5	8.0	29530	292	135	0.38	10
9	6.5	8.0	20049	241	107	0.38	8
9	6.5	8.0	22784	294	132	0.43	10
9	6.5	8.0	22544	268	123	0.38	10
9	6.5	8.0	21603	252	107	0.39	10
9	6.5	8.0	19629	296	100	0.37	11
9	6.5	8.0	21257	277	94	0.37	9
9	6.5	8.0	20048	214	109	0.38	11
9	6.5	8.0	12696	191	98	0.43	6
9	6.5	8.0	14932	177	105	0.44	6
9	6.5	8.0	9953	103	108	0.50	4
9	6.5	8.0	17500	195	149	0.43	11
9	6.5	8.0	24230	234	144	0.39	3
9	6.5	8.0	14312	197	104	0.41	6
9	6.5	8.0	15615	187	126	0.40	4
9	6.5	8.0	16029	222	102	0.39	5
9	6.5	8.0	15095	166	141	0.47	5
10	6.5	1.5	78227	581	193	0.29	4
10	6.5	8.5	72759	445	224	0.29	8
10	6.5	8.5	87047	467	256	0.29	12
10	6.5	8.5	77170	514	204	0.24	11
10	6.5	8.5	64662	413	208	0.24	9
10	6.5	12.0	51574	479	136	0.25	9
10	6.5	12.0	33781	341	122	0.30	4
10	6.5	12.0	72498	479	195	0.25	6
10	6.5	12.0	61995	432	170	0.25	2
11	6.7	11.6	21984	227	126	0.41	9
11	6.7	11.6	19935	197	124	0.45	8
11	6.7	11.6	24231	219	138	0.35	7
11	6.7	8.4	28737	281	134	0.32	4
11	6.7	8.4	35973	265	173	0.34	8

11	6.7	8.4	33311	270	160	0.32	5
11	6.7	8.4	25238	233	149	0.36	7
11	6.7	8.4	19274	222	115	0.32	2
11	6.7	8.4	37857	291	177	0.31	5
13	18.0	17.8	149523	928	214	0.19	6
13	18.0	17.8	122414	650	225	0.20	8
13	18.0	17.8	117254	639	221	0.19	6
13	18.0	17.8	47618	567	119	0.27	4
14	18.0	17.3	31858	551	92	0.33	8
14	18.0	17.3	31071	270	130	0.31	9
14	18.0	17.3	45733	419	165	0.32	5
14	18.0	17.4	45409	633	93	0.23	5
14	18.0	17.4	54919	515	149	0.24	5
14	18.0	17.4	55223	577	130	0.26	7
14	18.0	17.4	17083	175	118	0.35	3
14	18.0	17.4	68118	612	138	0.21	12
14	18.0	17.4	84981	641	171	0.22	13
14	18.0	17.4	44585	458	128	0.27	7
14	18.0	17.4	33850	382	115	0.27	5
14	18.0	17.4	30882	246	149	0.29	2
14	18.0	17.4	28250	286	116	0.30	4
15	18.2	18.9	60341	537	151	0.23	6
15	18.2	18.9	22623	178	159	0.36	7
15	18.2	14.7	38852	277	163	0.27	6
15	18.2	14.7	32650	276	165	0.36	5
15	18.2	14.7	23458	190	127	0.33	3
15	18.2	14.7	40653	307	163	0.28	8
15	18.2	14.7	19735	350	72	0.31	2
16	18.3	36.6	47821	510	122	0.24	2
16	18.3	36.6	46239	552	114	0.25	3
16	18.3	36.6	32081	525	84	0.29	2
17	18.4	29.8	106352	810	197	0.23	0

References

1. Zheng X, Ye H, Tang Y. Image Bi-Level Thresholding Based on Gray Level-Local Variance Histogram. *Entropy*. 2017;19:191.
2. Emde B, Heinen A, Gödecke A, Bottermann K. Wheat germ agglutinin staining as a suitable method for detection and quantification of fibrosis in cardiac tissue after myocardial infarction. *Eur J Histochem*. 2014;58:2448.
3. Eilers PHC, Goeman JJ. Enhancing scatterplots with smoothed densities. *Bioinformatics*. 2004;20:623–628.
4. Engelman ZJ, Trew ML, Smaill BH. Structural heterogeneity alone is a sufficient substrate for dynamic instability and altered restitution. *Circ Arrhythm Electrophysiol*. 2010;3:195–203.
5. Yushkevich PA, Piven J, Hazlett HC, Smith RG, Ho S, Gee JC, Gerig G. User-guided 3D active contour segmentation of anatomical structures: Significantly improved efficiency and reliability. *Neuroimage*. 2006;
6. Reyment RA, Jvreskog KG. Applied Factor Analysis in the Natural Sciences. 1993.
7. Legland D, Kiêu K, Devaux M-F. Computation of minkowski measures on 2D and 3D binary images. *Image Anal Stereol*. 2011;26:83.